Spectrochemical analyses of growth phase-related bacterial responses to low (environmentally-relevant) concentrations of tetracycline and nanoparticulate silver

Naifu Jin[1], Kirk T. Semple[1], Longfei Jiang[2], Chunling Luo[2], Dayi Zhang[1,3,*], Francis L. Martin[4,*]

[1]*Lancaster Environment Centre, Lancaster University, Lancaster LA1 4YQ, UK;*

[2]*Guangzhou Institute of Geochemistry, Chinese Academy of Sciences, Guangzhou 510640, China;*

[3]*School of Environment, Tsinghua University, Beijin 100084, China;*

[4]*School of Pharmacy and Biomedical Sciences, University of Central Lancashire, Preston PR1 2HE, UK;*

***Corresponding authors:**

Francis L Martin, School of Pharmacy and Biomedical Sciences, University of Central Lancashire, Preston PR1 2HE, UK; Email: flmartin@uclan.ac.uk

Dayi Zhang, School of Environment, Tsinghua University, Beijin 100084, China; Email: d.zhang@lancaster.ac.uk

Abstract

Exposure to environmental insults generally occurs at low levels, making it challenging to measure bacterial responses to such interactions. Additionally, microbial behaviour and phenotype varies in differing bacterial types or growth phases, likely giving rise to growth- or species-specific responses to environmental stimuli. The present study applied a spectrochemical tool, infrared (IR) spectral interrogation coupled with multivariate analysis, to investigate the growth- and species-specific responses of two bacterial strains, Gram-negative *Pseudomonas fluorescens* and Gram-positive *Mycobacterium vanbaalenii*, to low concentrations of tetracycline, nanoparticulate silver (AgNP) or mixtures thereof. Results indicate the tendency for tetracycline-induced biospectral alterations to occur in outer-cellular components, *e.g.*, phospholipids or proteins, while AgNPs-induced changes are mainly associated with proteins (~ 964 cm^{-1}, ~ 1485 cm^{-1}, ~ 1550 cm^{-1}, ~ 1650 cm^{-1}). The primary altered targets are correlated with bacterial membranes or outer-cellular components. Furthermore, significant lipid changes at 1705-1750 cm^{-1} were only present in *P. fluorescens* cells compared to *M. vanbaalenii*, owing to differences in cell wall structure between Gram-positive and -negative bacteria. This study also found distinct biospectral alterations in non-log phase compared to log phase, confirming bacterial growth-dependent responses to environmental exposures. It implies that previous studies on log phase only may underestimate the impacts from exposures of interest *in situ*, where bacteria stay in different growth stages. Our work proves the feasibility of biospectroscopy in determining bacterial responses to low-level environmental exposures in a fast and efficient manner, revealing sufficient biochemical information continuously through growth phases. As a nondestructive approach, biospectroscopy may provide deeper insights into the actual and *in situ* interactions between microbes and environmental stimuli, regardless of the exposure level, growth phase, or bacterial types.

50 **ToC graphic**

51

52

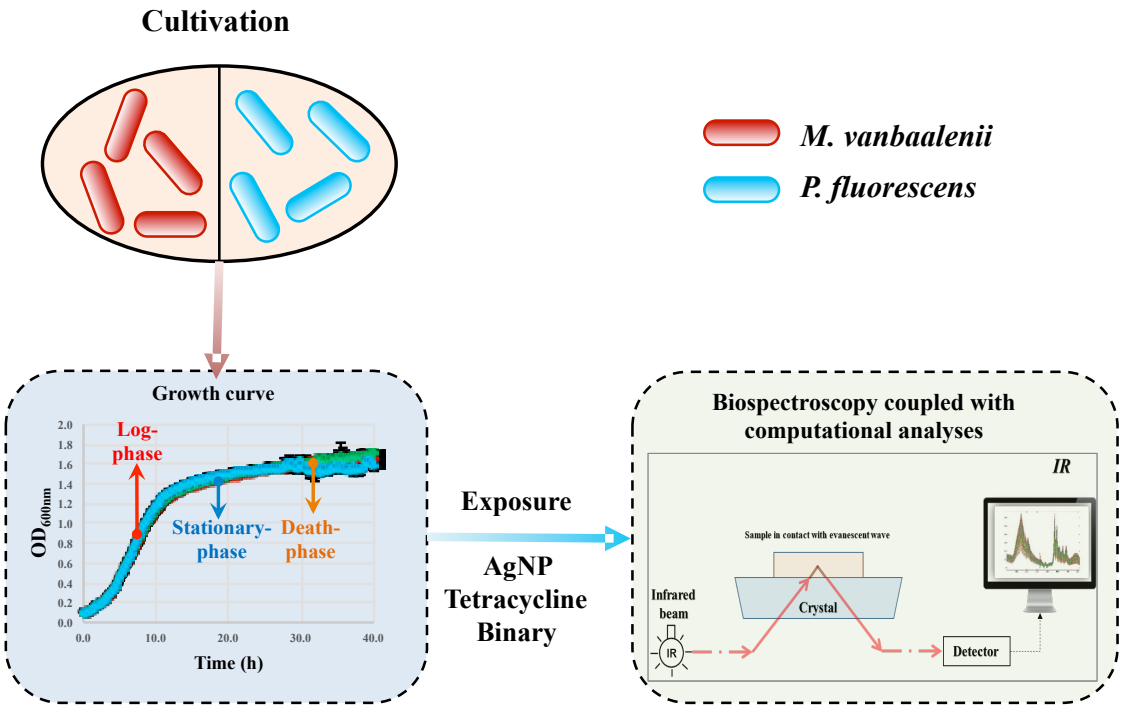

53
54

Introduction

The impacts of environmental insults on microorganisms have been widely studied. Antibiotics are a group of antimicrobial agents capable of causing environmental insults of major concern from both a scientific and public perspective. A significant number and quantity of antibiotics have been extensively applied in human and veterinary medicine[1]. Various means by which these drugs and their metabolites enter the environment post-excretion have been examined. The most common way by which antibiotics are discharged is *via* sewage treatment plants with ultimate release into surface or groundwater. Previous studies point to >40 different categories of antibiotics found in groundwater and even drinking water, ranging from nanogram per liter to microgram per liter[1-4]. Strikingly, residues of veterinary antibiotics enter the environment in a much more direct way through application of liquid manure as fertilizer[5, 6].

Additionally, nanoparticles (NPs) may also pose high risks to our living environment. Nanoparticulate silver (AgNP) is one of the most widely-used NPs, occurring in analytical pathogen-detecting devices, as antibacterial additives in commercial products (clothing, food containers, wound dressings, implant coatings, and refrigerators), and in ultrafiltration membranes for water purification[7-9]. The abuse and widespread usage of antibiotics and AgNPs may exacerbate risks of antimicrobial resistance[10]. Although many studies have addressed such consequences in living microorganisms, they usually employ very high-level exposures of antibiotics and AgNPs in the laboratory, generally 100- or even 1000-fold greater than exposures in real-world scenarios. Thus, the *in-vitro* outcome of high-level exposure in reflecting real-world impacts is always questioned[11, 12].

Bacteria play a critical role in geochemical processes and are ubiquitously present in the environment as a unique group of microorganisms. They can be used advantageously to study the impacts of environmental exposures, but their communities are incredibly complicated with regards to composition, functions and dynamics[13-16]. Gram staining depending on cell membrane structure, for instance, is the general classification method for categorizing bacteria into Gram-positive or -negative groupings. The fundamental difference between these two categories is membrane structure, *i.e.*, there is only a thin peptidoglycan layer (~2-3 nm) between the cytoplasmic membrane and the outer membrane of Gram-negative bacteria while

Gram-positive bacteria exhibit a thick peptidoglycan layer of 30 nm but lack an outer membrane[17]. Differing attributes of membrane structure may result in distinct responsive behaviors towards environmental exposures, for instance towards toxicity and anti-biocide actions[18]. Additionally, growth phase is another major concern in studying bacterial communities. Bacterial growth is typically divided *via* growth rate, *i.e.*, lag phase, acceleration phase, exponential phase (log-phase), retardation phase, stationary phase, and phase of decline. In previous studies, log-phase has been the most investigated, but this condition is seldom found in the natural environment due to rarity of optimal growth conditions[19]. Instead, stationary- to death-phase representing nutrient depletion circumstances may be more representative[20].

To date, a wide range of techniques have been used to assess bacterial responses to environmental exposures, such as Christensen test-tube method (CTT)[21, 22], Congo red agar method (CRA)[23], IcaADB gene detection using polymerase chain reaction (PCR)[24, 25], and pulsed-field gel electrophoresis (PFGE)[26, 27]. However, these approaches target specific endpoints and are not feasible for diagnosing bacterial responses to environmental exposures. CTT and CRA primarily require access to pure cultures. The others are molecular-based, defining the genotype of a whole community rather than the individual phenotype or behavior. For instance, distinguishing the functions or behaviours of individual bacterial cells within a bacterial biofilm is almost impossible *via* molecular-based methods, owing to the enormous diversity of bacterial strains and complexity in community structure. Additionally, these approaches have to be performed under restrictive laboratory conditions[28-30], making it unachievable to discriminate bacterial phenotypes within complex bacterial communities in real environmental samples. Therefore, an increasing need for novel high-throughput approaches is raised, allowing one to analyze the real environmental microbiota *in situ via* a non-destructive means.

Biospectroscopy has a long history of application in microbiology since the 1960s[31, 32]. Attributes of biospectroscopy include non-destructive, non-invasive, high-throughput and label-free, which provide many advantages for the investigation of environmental and biochemical dynamic changes in low-level exposure circumstances. In recent studies, biospectroscopy has proved sensitive to physiological and morphological alterations resulted from low-level environmental exposures[33-35]. Specifically, infrared (IR) spectroscopy exploits the principle that

biochemical bonds perform some degree of vibrations induced by stretching, bending, scissoring or twisting after energy absorption at particular wavelengths. The "biochemical-cell fingerprint" region is located within the mid-IR region, which is the most information-rich about biochemical structures[36]. Through assessing derived spectral peaks or alterations, *i.e.*, bio-fingerprints, the biochemical structure of interrogated targets can be revealed[37-39]. Additionally, Raman spectroscopy, as a complementary method to IR, can provide information on chemical bonds and composition even under a hydrated environment[40, 41]. Furthermore, another merit of biospectroscopy over other techniques is that it allows investigations to be undertaken *in situ* in real-time, which can generate continuous biochemical information through the entire biological processes rather than only obtaining static results from specific time points.

As a broad-spectrum of antibiotic, tetracycline is effective against both Gram-positive and -negative bacteria with only a few exceptions[42], having a history of several decades usage in animal feeds and consequently probably more ubiquitous in the natural environment than other in-house antibiotics (*e.g.*, kanamycin)[43]. The present study therefore chose tetracycline as the studied antibiotic, discriminating and assessing bacterial responses to tetracycline and AgNPs *via* biospectroscopy coupled with multivariate analysis. Additionally, recent studies have reported the synergistic antibacterial effects of antibiotics and metals or NPs[44], *e.g.*, amoxicillin and AgNPs [45], but its effects on bacterial physiology remains unclear. Our work also considered and interrogated microbial responses to the binary-exposure of tetracycline and AgNPs *via* IR spectroscopy. Regarding the real-world scenario, our results distinguished the distinct biospectral alterations in different bacterial types and growth phases, helping one to understand the bacterial behaviour post-exposure to low-level antimicrobials. We aim to demonstrate that biospectroscopy approaches can characterise physiological features of bacteria and lend profound insights into the relationship between these and bacterial responses to environmental insults.

Materials and methods

Sample preparation

Unless stated otherwise, all the chemicals used in this study were purchased from Sigma-Aldrich (UK). The AgNPs (catalogue no. 730785, Sigma-Aldrich, UK) have a 10-nm particle size at a stock concentration of 0.02 mg/mL, dissolved in aqueous buffer with sodium citrate as stabilizer. Two classic soil bacterial strains, *Mycobacterium vanbaalenii* PYR-1 (Gram-positive) and *Pseudomonas fluorescens* (Gram-negative), were selected owing to their ubiquity and wide distribution in the soil environment and their well-known physiological behaviour[36, 46-48]. These two strains were cultured in Luria-Bertani (LB) broth at 30±2^{o}C with 150 rpm shaking for 24 h. Bacterial growth was measured every 10 min by optical density at 600 nm (OD_{600}) with a microplate reader (FLUOstar Omega, BMG Labtech, UK). AgNPs, tetracycline or AgNPs-tetracycline mixture was added into cell suspensions in early log-phase (OD_{600}=0.6), respectively. To mimic the low-level exposure in natural environment[49-52], the exposure concentration was set as 4 μg/L for AgNPs and 1 μg/L for tetracycline. One millilitre of bacterial suspension was taken 2, 8 and 24 h post-exposure, representing log-phase, stationary-phase and death-phase, respectively. For each sample, bacterial cells were harvested by centrifugation at 4000 relative centrifugal force (rcf) for 5 min, and the cell pellets were subsequently washed three times with sterile deionized water and 70% ethanol to fix bacteria and remove residues of growth media. The fixed samples were then applied onto Low-E slides for subsequent spectrochemical analysis.

Spectrochemical analysis

IR spectra were acquired *via* a Bruker TENSOR 27 FTIR spectrometer (Bruker Optics Ltd., UK) equipped with a Helios ATR attachment containing a diamond internal reflection element (IRE). Instrument parameters were set at 32 scans and 16 cm^{-1} resolution. A total number of 30 spectra were acquired per sample through the ATR magnification-limited viewfinder camera. Before measuring each new specimen, the crystal was cleaned with deionized water, and background readings were retaken.

Raman spectra were acquired *via* an InVia Renishaw Raman spectrometer (Renishaw Inc. Gloucester, Gloucestershire, UK). After calibration, sample slides were placed on an operating stage (a Renishaw automated 100 nm encoded XYZ

stage), and a 50× objective (numeral aperture 0.75) was applied to focus on the cell pellet. The parameters of measurement included: grating scan type (extended); spectrum range (400 to 1800 cm^{-1}); configuration (Laser, 785 nm edge); grating (1200 l/mm 633/790); exposure time (30 s); accumulations (1); and, laser power (100%). When all the parameters were set up, a map measurement was used for analyzing each colony. The spectrometer's entrance slit of 50 μm combined with a 1200 lines/mm (~1.0 cm^{-1} spectral resolution) diffraction grating dispersing Raman signals onto a master Renishaw Pelletier cooled charge coupled detector (CCD). A white light camera mounted on the microscope was used to obtain the darkfield images and visualize locations for spectral acquisition. For each captured picture of a cell pellet, 25 spectra were randomly obtained.

Spectrochemical data processing

All the initial data generated from ATR-FTIR spectroscopy were analyzed using MATLAB R2011a (TheMathsWorks, Natick, MA, USA) coupled with the IRootLab toolbox (http://irootlab.googlecode.com)[53]. The acquired IR spectra were cut to the biochemical-cell fingerprint region (1800 - 900 cm^{-1}), undertaken rubberband baseline correction and normalized to Amide I (1650 cm^{-1}). Multivariate analysis of principal component analysis-linear discriminant analysis (PCA-LDA) was applied to the pre-processed data to derive ten uncorrelated principal components (PCs) from acquired spectra, which account for >99% of the total variance and also maximize inter-class variance whilst minimizing intra-class variance[54-56]. Cross-calculation was subsequently performed to mitigate risk resulting from LDA overfitting[57]. The PCA-LDA loadings using (n-1) samples (n = number of samples in dataset) was trained *via* leave-one-out cross-validation and then calculated the scores of the rest sample. This process was performed for all scores within the test. To investigate roles of reactive oxygen species (ROS) in antibiotic action and resistance, the CySS-to-protein ratio was calculated from derived Raman spectra by dividing the intensity of cysteine band (CySS, 668 cm^{-1}) by that of protein band (1447 cm^{-1})[34].

Statistical analysis

Statistical significance of differences and variance analysis (P-value <0.05) of biospectral alterations among different treatments of bacterial types and growth phases was performed using one-way analysis of variance (ANOVA) with Tukey's

post-hoc test. All statistical analyses were carried out in GraphPad Prism 6. Multivariate regression trees (MRT) were used to analyze the influence of bacterial type, growth phase and exposure on biospectral alterations using the R package "mvpart". Herein, Gram-positive (*M. vanbaalenii*) and Gram-negative (*P. fluorescens*) strains were assigned as 1 and 0. For growth phase, the log-phase, stationary-phase, and death-phase were assigned as 1, 2 and 3, respectively. The exposure of AgNPs, tetracycline and their mixtures were assigned as 1, 2 and 3, respectively.

Results and discussion

Growth curves post-exposure to AgNPs and tetracycline

Growth curves (Figure 1) for *M. vanbaalenii* (Figure 1A) and *P. fluorescens* (Figure 1B) show that both strains exhibit approximately a 3 h lag-phase and the log-phase starts some 3.5 h after initial culture. Both enter the stationary-phase at approximately 11 h (OD_{600}=1.2). After about 30 h culture, significant fluctuations indicate the death phase stage for both strains. There was no significant difference regarding the growth between control (non-exposure) and exposure groups (P >0.05). Although previous work reports a remarkable inhibition of bacterial growth post-exposure to AgNPs[58], the exposure levels herein (4 ng/mL) are much lower than the previous study (10-100 μg/mL) and it therefore appeared not to significantly impact either bacterial strain. Similarly, low concentrations of tetracycline did not induce any apparent changes on the respective growth curves either. A previous study reports that *Synechocystis* sp. exposure to 1 μg/L of tetracycline for five days exhibited no apparent effect, possibly because of natural variability in tetracycline resistance[59]. Additionally, *M. vanbaalenii* and *P. fluorescens* are both environmental bacteria widespread in natural habitats (water and soil), and they are reported to tolerate insults from low-level exposures of antimicrobials[36]. Thus, their growth curves are hardly affected by low-level exposures to AgNPs or tetracycline.

Growth-dependent spectrochemical alterations derived from IR spectra

Raw spectra reveal very limited information because low-level exposures may only induce miniscule alterations (Figure 1C and 1D). Multivariate analysis assists in highlighting the spectral changes and key distinguishing biomarkers representing

spectral differences. Previous studies indicate that most features align along linear discriminant one (LD1), which includes most of the spectral information (Figure 2)[34, 36]. The observed segregation in PCA-LDA scores plots (Figure 2A and 2E) is significant (P <0.05), indicating distinct biospectral alterations between the growth phases. The results of one-way ANOVA [see Electronic Supporting Information (ESI) Table S1 and S2] also demonstrate the statistically significant means of all segregation categories in each growth phase (P <0.05).

Biospectral discriminant peaks and their tentative assignments illustrate the interactions between cellular components in different growth stages (Figure 3). The spectra of *M. vanbaalenii* show a broad range of variations in stationary-phase compared to log-phase (Figure 3A), including glycogen (~1018 cm^{-1}), carbohydrate (~1165 cm^{-1}), symmetric phosphate stretching vibrations ($\nu_s PO_2^-$; ~1088 cm^{-1}), COO- symmetric stretching vibrations of fatty acids and amino acid (~1377 cm^{-1}), lipid (~1701 cm^{-1}), and proteins (~1474 cm^{-1})[60]. The main discriminant peaks in death-phase include Amide I (~1650 cm^{-1}), Amide II (~1550 cm^{-1}), glycogen (~1018 cm^{-1}), and proteins (~1481 cm^{-1})[36, 60]. In contrast, the major spectral features of *P. fluorescens* are identical in stationary-phase and death-phase (Figure 3E), mainly comprising proteins and lipids, *i.e.*, Amide I (~1650 cm^{-1}), Amide II (~1550 cm^{-1}), and lipids (1705-1750 cm^{-1})[34, 35]. For both strains, the degrees of all the growth-related alterations illustrate an increasing tendency from stationary-phase to death-phase, possibly attributed to cellular differentiation under nutrient depleted conditions in stationary-phase and death-phase, which cause the changing cell wall structure to adapt to growth circumstances[20, 61, 62]. The spectral differences between the two strains is principally contributed by cell membrane structure in that Gram-negative bacteria contain two lipid-associated bilayers compared to Gram-positive cells[17]. The extra membrane in Gram-negative strains (*P. fluorescens*) might increase more detectable alterations related to proteins and lipids across growth phases.

Spectrochemical alterations with AgNPs/tetracycline exposure

Although the exposures herein are low-level, characterizable effects can be identified post-exposure to AgNPs, tetracycline or their mixtures *via* biospectrsocopy coupled with multivariate analysis. The key alterations in *M. vanbaalenii* post-exposure to AgNPs include glycogen (~1022 cm^{-1}), proteins (~1485 cm^{-1}), $\nu_s PO_2^-$ (~1088 cm^{-1},

1092 cm^{-1}), carbohydrate (~1165 cm^{-1}), lipids (~1705 cm^{-1}, 1709 cm^{-1}), Amide I (~1670 cm^{-1}), and protein phosphorylation (~964 cm^{-1}) (Figure 3B)[33, 36]. Tetracycline exposure led to discriminating alterations in *M. vanbaalenii* in Amide III (~1269 cm^{-1}), protein phosphorylation (~964 cm^{-1}), glycogen (~1022 cm^{-1}), Amide I (~1609 cm^{-1}, 1612 cm^{-1}, 1659 cm^{-1}), COO- symmetric stretching vibrations of fatty acids and amino acid (~1408 cm^{-1}), and lipids (~1701 cm^{-1}, 1713 cm^{-1})[60] (Figure 3C). However, for *P. fluorescens*, the biomarkers in both individual treatments are further concentrated on proteins (~1650 cm^{-1}, ~1550 cm^{-1}) and lipids (1705-1750 cm^{-1})[34, 36] (Figure 3F and 3G).

In binary exposure treatments, more complex profile differences in spectral alterations in ATR-FTIR spectra are observed. The primary changes in *M. vanbaalenii* are consistent with proteins (~1650 cm^{-1}) and lipids (1705-1750 cm^{-1}) in all growth phases (Figure 3D)[34, 36]. In contrast, the exposure-associated spectral alterations in *P. fluorescens* vary significantly with growth phase (Figure 3H), *e.g.*, the biomarkers in stationary-phase with binary effects include glycogen (~1053 cm^{-1}), Amide I (~1609 cm^{-1}), COO- symmetric stretching vibrations of fatty acids and amino acid (~1389 cm^{-1}), asymmetric phosphate stretching vibrations ($\nu_{as}PO_2^-$; ~ 1196 cm^{-1}), lipid (~ 1732 cm^{-1}), and Amide II (~1508 cm^{-1})[35, 60]. They change to lipid (~1709 cm^{-1} and 1751 cm^{-1}), Amide I (~1609 cm^{-1}), Amide II (~1543 cm^{-1}), $\nu_{as}PO_2^-$ (~1211 cm^{-1}) and glycogen (~1053 cm^{-1})[36, 60] in death-phase.

In general, most spectral alterations post-exposure are associated with lipids and proteins indicating bacterial cell membranes are primary targets, probably because tetracycline or AgNPs penetrate bacterial cells *via* passive diffusion and inhibits bacterial growth by disturbing protein synthesis or altering membrane structure[63]. Through growth phases, Gram-negative bacteria inhibit a broad range of alterations associated with lipids, *e.g.*, (1705 − 1750 cm^{-1}), which is absent in Gram-positive bacteria, mainly attributed to their different cell wall composition. The rigidity and extended cross-linking may reduce target sites on cell wall for environmental exposure and increase difficulties in antimicrobial penetration[44].

Factors influencing spectrochemical alteration

From conducted spectral analysis, factors inducing IR spectral alterations can be classified as intrinsic and external categories. The inherent one includes bacterial type

(Gram-positive or Gram-negative) and growth phase, and the external category refers to the types of exposure. These factors function and interact simultaneously, with distinct impacts on microbial responses to environmental exposures. To quantify the importance of each factor, multivariate regression tree (MRT) analysis was conducted through the isolated discriminating biomarkers (characteristic peaks). The MRT graph illustrates the relationship of spectral variations and impact factors with four splits according to bacterial types, growth phase and exposure groups, explaining 90.8% of spectral variance (Figure 5).

Spectral variation is first split by bacterial type which accounts for 65.6% of the total variation, owing to more changes associated with membrane components observed in *P. fluorescens* (Gram-negative) than *M. vanbaalenii* (Gram-positive), *e.g.*, proteins and phospholipid-derived fatty acids. Multivariate analysis also illustrates various spectrochemical alterations between *P. fluorescens* and *M. vanbaalenii*. For example, significant lipid changes (1705-1750 cm^{-1}) present in *P. fluorescens* treatments are absent in *M. vanbaalenii* treatments. The cell membrane of Gram-negative bacteria contains two lipid associated bilayers, which is likely to increase the influence of applied exposure on the cell wall structure, while there is only one lipid bilayer in the membrane and a thick ring of peptidoglycan and teichoic acid of Gram-positive bacteria[17]. This difference may influence the structural integrity and eventually the microbial response to external stimuli. Furthermore, both Gram-positive and -negative bacteria from stationary phase show a comprehensive range of alterations in cellular components (*i.e.*, Amide I, II, III, $\nu_{as}PO_2^-$/ $\nu_sPO_2^-$, glycogen, carbohydrates, lipids, etc.; Figure 6), indicating many underlying biological activities. This can be primarily attributed to a growing cell wall from log to stationary phase, which increases the amounts of membrane components[64] and induces changes on the surface of the bacterial envelope and protein synthesis[20]. Such changes may have considerable influence on the rigidity of the cells, resistance to environmental changes, as well as immunochemical properties. Results of both MRT and multivariate analyses therefore suggest bacterial type as the primary intrinsic factor determining IR alterations post-exposure to AgNP or tetracycline.

Growth phase also shows significant impacts on bacterial spectra after environmental exposure. The Gram-negative group is further split in the MRT graph by growth phase (*i.e.*, log-phase *vs.* stationary-phase and death-phase), owing to

increasing alterations of membrane components along with the growth stage, which explains 13.2% of total variation (Figure 5). Similarly, multivariate analysis demonstrates the same growth-dependent results. Post-exposure to AgNP for instance, the spectra of both strains in log-phase are clearly separated from those in stationary-phase or death-phase (Figure 2B-D). The induced alterations from growth phases are associated with various cellular components. Specifically in log-phase, IR spectral biomarkers reflecting the major alterations of *M. vanbaalenii* post-exposure to AgNP are Amide I (~1612 cm^{-1}), COO- symmetric stretching vibrations of fatty acids and amino acids (~1381 cm^{-1}), lipid (~1717 cm^{-1}), glycogen (~1011 cm^{-1}), $\nu_{as}PO_2^-$ (~1215 cm^{-1}), and carbohydrate (~1165 cm^{-1}) (Figure 6A)[36, 60]. However, samples from stationary-phase exhibit a contrasting profile consisting only of alterations of proteins (~1377 cm^{-1}) and Amide I, II, III (~1609 cm^{-1}, 1566 cm^{-1}, 1254 cm^{-1}) (Figure 6B)[33]. In tetracycline or tetracycline-AgNP mixture treatments, the most-induced biomarkers in log-phase shift to proteins, *i.e.*, Amide I (~1163 cm^{-1}, 1616 cm^{-1}), Amide II (~1520 cm^{-1}, 1558 cm^{-1}) and Amide III (~1327 cm^{-1}) (Figure 6A)[33], but they are associated more with cellular components in stationary-phase, including Amide I (~1589 cm^{-1}), Amide II (~1551 cm^{-1}), Amide III (~1269 cm^{-1}; 1273 cm^{-1}), proteins (~1485 cm^{-1}), lipid (~1717 cm^{-1}, 1721 cm^{-1}), COO- symmetric stretching vibrations of fatty acids and amino acid (~1342 cm^{-1}; 1381 cm^{-1}), $\nu_sPO_2^-$ (~1069 cm^{-1}), $\nu_{as}PO_2^-$ (~1196 cm^{-1}) and glycogen (~1018 cm^{-1}) (Figure 6B)[60]. Samples from death-phase cultures exhibit distinct patterns as compared to log- or stationary-phase in that AgNP and tetracycline-AgNP mixture show more impacts on proteins (Figure 6C). These results indicate the changing physiological profiles of bacterial cells with growth stage, and the different modifications associated with cellular components with adaptation to the living environment. For instance, bacteria facing nutrient depletion are reported to produce more hydrophobic molecules to protect the starved cells, resulting in less fluid and permeable membranes attributed to the transformations within the fatty acid composition, which increase protection and insulation from a stressful environment[20, 61, 62]. Moreover, entering stationary phase, a wide range of protein synthesis is also altered by the global gene regulatory network, which tends to swap the core functions from metabolism or catabolism to the maintenance of cellular viability[20], possibly explaining more spectral alterations of proteins in stationary- and death-phase than log-phase.

Besides intrinsic factors, external environmental exposure explains 12.0% of total variation in MRT for Gram-positive (2.7%) and Gram-negative (9.3%) bacteria. For both strains, segregation mainly results from different spectrochemical alterations between AgNP exposure and tetracycline/binary groups. The key spectral alterations in the AgNP category are located at COO- symmetric stretching vibrations of fatty acids and amino acid (~1373 cm^{-1}), (~1736 cm^{-1}), proteins (~984 cm^{-1}, 988 cm^{-1}), Amide I (1612 cm^{-1}, 1694), Amide II (1543 cm^{-1}, 1562 cm^{-1}), and $\nu_s PO_2^-$ (1088 cm^{-1}) (Figure 3B and 3F)[36, 60]. In contrast, changes induced by tetracycline or tetracycline-AgNP mixture are associated with COO- symmetric stretching vibrations of fatty acids and amino acid (~1373 cm^{-1}), proteins (~984 cm^{-1}), lipids (~1697 cm^{-1}; 1732 cm^{-1}), and Amide I, II (~1562 cm^{-1}, 1616 cm^{-1}) (Figure 3C and 3G)[60].

It can be concluded that AgNP-induced spectral changes are mainly associated with proteins, whereas broader cellular components are affected post-exposure to tetracycline or tetracycline-AgNP mixture. It might be explained by tetracycline penetrating cells *via* passive diffusion, which alters bacterial growth by inhibiting protein synthesis or destroying the membrane. Phospho-lipids or proteins are therefore more significantly affected as the primary receptors of passively accumulated tetracycline[63]. Although mechanisms of AgNP interacting with cytoplasmic membranes and penetrating into cells remain unclear[58, 65], our data suggest that AgNP-induced alterations might be derived from some specific active sites interacting with AgNP, *e.g.*, sulfur-containing proteins following a similar mechanism as thiol groups of respiratory chain proteins and transport proteins[66-68].

To further assess the impact of exposure, the inter-category multivariate distances of each category were also evaluated. PCA-LDA scores plots that compare the spectrochemical alterations of the two bacterial strains within the same growth phase are shown in Figure 4. The results illustrate distinct clustering of tetracycline exposure away from the control category, but not for AgNP categories, whereas the binary group is located between AgNP and tetracycline categories. The spectral differences of *M. vanbaalenii* between categories of control and binary exposure are slightly reduced within 0.1 as compared to the tetracycline exposure category, indicating that AgNP may confer the exposure effect of tetracycline. Similar alterations are observed for *P. fluorescens*. Additionally, for both *M. vanbaalenii* and *P. fluorescens*, the AgNP and tetracycline categories in the stationary- or death-phase

shift in an opposite direction from the control, and the binary exposure category locates closer to the tetracycline exposure group than control or AgNP exposure. This finding is supported by a range of identical alterations identified in both AgNP and binary exposure groups from stationary-phase to death-phase (*i.e.*, lipids, Amide I, II, III, $\nu_{as}PO_2^-$/ $\nu_sPO_2^-$).

Additionally, the analysis of reactive oxygen species (ROS) was also conducted to evaluate the exposure impacts by calculating the CySS-to-protein ratio, derived from Raman spectra (Figure 7), which points to cellular ROS levels[34]. Interestingly, comparing to control category, only tetracycline-binary exposure appears to increase ROS level (P <0.05), whereas the induction of AgNP and tetracycline exposure is not significant. Previous studies report the independent mechanisms of antimicrobials on the involvement of ROS[69, 70]. The results herein hint at no ROS generation from individual AgNP or tetracycline exposure, and the spectrochemical alterations more likely result from the direct inhibition of cell-wall assembly, protein synthesis and DNA replication. In binary exposure, AgNP penetration across the cell membrane might increase permeability and result in more tetracycline entering the bacterial cell, consequently triggering a ROS response[44, 71-74].

Conclusions

The present study demonstrates that spectrochemical techniques coupled with multivariate analysis are a robust tool for investigating the bacterial response to environmental exposures, revealing biochemical information longnitudinally at low-level exposures. This approach can be applied to characterize and assess bacterial alterations effectively post-exposure to a tetracycline and/or AgNP through growth phases and is potentially feasible for *in situ* interrogation of antimicrobial effects in real-time. Deeper insights into biospectral alterations in non-log phases pertaining nutrient depletion conditions, which fits better with the real-world scenario of microcosms, uncovers the distinct changes of biochemical fingerprints across growth periods, hinting at an underestimation of antimicrobial effects in previous studies. Bacterial type is ranked as the primary factor affecting microbial response to environmental stimuli by MRT analysis, followed by growth phase and types of antimicrobials. These findings will help our better understanding of the real interactions between microbes and low-level antimicrobials under natural environmental conditions, *e.g.*, nutrient depletion.

Conflicts of interest

There are no conflicts of interest to declare.

Acknlowledgement

N.J. was funded by Chinese Academy of Sciences and China Scholarship Council.

References

1. G. Hamscher, S. Sczesny, H. Höper and H. Nau, *Analytical Chemistry*, 2002, **74**, 1509-1518.
2. T. S. TA, *Quintessence Int.*, 1998, **29**, 223-229.
3. J. C. Chee-Sanford, R. I. Aminov, I. J. Krapac, N. Garrigues-Jeanjean and R. I. Mackie, *Applied and Environmental Microbiology*, 2001, **67**, 1494-1502.
4. L. Cantas, S. Q. Shah, L. M. Cavaco, C. M. Manaia, F. Walsh, M. Popowska, H. Garelick, H. Burgmann and H. Sorum, *Frontiers in Microbiology*, 2013, **4**, 96.
5. M. Tandukar, S. Oh, U. Tezel, K. T. Konstantinidis and S. G. Pavlostathis, *Environmental Science and Technology*, 2013, **47**, 9730-9738.
6. J. L. Martinez and F. Baquero, *Upsala Journal Medical Sciences*, 2014, **119**, 68-77.
7. H. H. Lara, N. V. Ayala-Núñez, L. d. C. Ixtepan Turrent and C. Rodríguez Padilla, *World Journal of Microbiology and Biotechnology*, 2009, **26**, 615-621.
8. R. J. Griffitt, N. J. Brown-Peterson, D. A. Savin, C. S. Manning, I. Boube, R. A. Ryan and M. Brouwer, *Environmental Toxicology and Chemistry*, 2012, **31**, 160-167.
9. Y. Kampmann, E. De Clerck, S. Kohn, D. Patchala, R. Langerock and J. Kreyenschmidt, *Journal of Applied Microbiology*, 2008, **104**, 1808-1814.
10. A. Gupta and S. Silver, *Nature Biotechnology*, 1998, **16**, 888-888.
11. O. I. Kalantzi, R. Hewitt, K. J. Ford, L. Cooper, R. E. Alcock, G. O. Thomas, J. A. Morris, T. J. McMillan, K. C. Jones and F. L. Martin, *Carcinogenesis*, 2004, **25**, 613-622.
12. J. L. Barber, M. J. Walsh, R. Hewitt, K. C. Jones and F. L. Martin, *Mutagenesis*, 2006, **21**, 351-360.
13. E. K. Costello, C. L. Lauber, M. Hamady, N. Fierer, J. I. Gordon and R. Knight, *Science*, 2009, **326**, 1694-1697.

14. C. L. Lauber, M. Hamady, R. Knight and N. Fierer, *Applied and Environmental Microbiology*, 2009, **75**, 5111-5120.
15. P. Marschner, C.-H. Yang, R. Lieberei and D. Crowley, *Soil Biology and Biochemistry*, 2001, **33**, 1437-1445.
16. M. Wietz, B. Wemheuer, H. Simon, H. A. Giebel, M. A. Seibt, R. Daniel, T. Brinkhoff and M. Simon, *Environmental Microbiology*, 2015, **17**, 3822-3831.
17. J. R. Morones, J. L. Elechiguerra, A. Camacho, K. Holt, J. B. Kouri, J. T. Ramirez and M. J. Yacaman, *Nanotechnology*, 2005, **16**, 2346-2353.
18. S. M. Ede, L. M. Hafner and P. M. Fredericks, *Applied Spectroscopy*, 2004, **58**, 317-322.
19. J. Monod, *Annual Reviews in Microbiology*, 1949, **3**, 371-394.
20. R. Kolter, D. A. Siegele and A. Tormo, *Annual Reviews in Microbiology*, 1993, **47**, 855-874.
21. F. Růžička, V. Holá, M. Votava, R. Tejkalová, R. Horvát, M. Heroldová and V. Woznicová, *Folia Microbiologica*, 2004, **49**, 596-600.
22. F. Ruzicka, M. Horka, V. Hola and M. Votava, *Journal of Microbiological Methods*, 2007, **68**, 530-535.
23. T. Mathur, S. Singhal, S. Khan, D. Upadhyay, T. Fatma and A. Rattan, *Indian Journal of Medical Microbiology*, 2006, **24**, 25.
24. D. Klug, F. Wallet, S. Kacet and R. J. Courcol, *Journal of Clinical Microbiology*, 2003, **41**, 3348-3350.
25. P. Vasudevan, M. K. M. Nair, T. Annamalai and K. S. Venkitanarayanan, *Veterinary Microbiology*, 2003, **92**, 179-185.
26. E. Muñoz-Atienza, C. Araújo, R. del Campo, P. E. Hernández, C. Herranz and L. M. Cintas, *LWT-Food Science and Technology*, 2016, **65**, 357-362.
27. F. C. Tenover, R. D. Arbeit, R. V. Goering, P. A. Mickelsen, B. E. Murray, D. H. Persing and B. Swaminathan, *Journal of Clinical Microbiology*, 1995, **33**, 2233.
28. E. E. Vaughan, F. Schut, H. Heilig, E. G. Zoetendal, W. M. de Vos and A. D. Akkermans, *Current Issues in Intestinal Microbiology*, 2000, **1**, 1-12.

29. M. Espy, J. Uhl, L. Sloan, S. Buckwalter, M. Jones, E. Vetter, J. Yao, N. Wengenack, J. Rosenblatt and F. Cockerill, *Clinical Microbiology Reviews*, 2006, **19**, 165-256.
30. D. Klein, *Trends in Molecular Medicine*, 2002, **8**, 257-260.
31. J. Heber, R. Sevenson and O. Boldman, *Science*, 1952, **116**, ll.
32. K. Norris, *Journal of Hygiene*, 1959, **57**, 326-345.
33. M. J. Baker, J. Trevisan, P. Bassan, R. Bhargava, H. J. Butler, K. M. Dorling, P. R. Fielden, S. W. Fogarty, N. J. Fullwood, K. A. Heys, C. Hughes, P. Lasch, P. L. Martin-Hirsch, B. Obinaju, G. D. Sockalingum, J. Sule-Suso, R. J. Strong, M. J. Walsh, B. R. Wood, P. Gardner and F. L. Martin, *Nature Protocols*, 2014, **9**, 1771-1791.
34. J. Li, R. Strong, J. Trevisan, S. W. Fogarty, N. J. Fullwood, K. C. Jones and F. L. Martin, *Environmental Science and Technology*, 2013, **47**, 10005-10011.
35. F. L. Martin, J. G. Kelly, V. Llabjani, P. L. Martin-Hirsch, I. I. Patel, J. Trevisan, N. J. Fullwood and M. J. Walsh, *Nature Protocols*, 2010, **5**, 1748-1760.
36. K. A. Heys, M. J. Riding, R. J. Strong, R. F. Shore, M. G. Pereira, K. C. Jones, K. T. Semple and F. L. Martin, *Analyst*, 2014, **139**, 896-905.
37. J. Schmitt and H.-C. Flemming, *Int Biodeterior Biodegradation*, 1998, **41**, 1-11.
38. A. Bosch, D. Serra, C. Prieto, J. Schmitt, D. Naumann and O. Yantorno, *Applied Microbiology and Biotechnology*, 2006, **71**, 736-747.
39. J. J. Ojeda, M. E. Romero-González, R. T. Bachmann, R. G. Edyvean and S. A. Banwart, *Langmuir*, 2008, **24**, 4032-4040.
40. S. J. Clarke, R. E. Littleford, W. E. Smith and R. Goodacre, *Analyst*, 2005, **130**, 1019-1026.
41. N. Pradhan, S. K. Pradhan, B. B. Nayak, P. S. Mukherjee, L. B. Sukla and B. K. Mishra, *Research in Microbiology*, 2008, **159**, 557-561.
42. I. Chopra and M. Roberts, *Microbiology and Molecular Biology Reviews*, 2001, **65**, 232-260.

43. M. D. Barton, *Nutrition Research Reviews*, 2000, **13**, 279-299.

44. A. M. Fayaz, K. Balaji, M. Girilal, R. Yadav, P. T. Kalaichelvan and R. Venketesan, *Nanomedicine*, 2010, **6**, 103-109.

45. P. Li, J. Li, C. Wu, Q. Wu and J. Li, *Nanotechnology*, 2005, **16**, 1912.

46. S.-J. Kim, O. Kweon, R. C. Jones, J. P. Freeman, R. D. Edmondson and C. E. Cerniglia, *Journal of Bacteriology*, 2007, **189**, 464-472.

47. J.-S. Seo, Y.-S. Keum and Q. X. Li, *International Journal of Environmental Research and Public Health*, 2009, **6**, 278-309.

48. L. S. Thomashow and D. M. Weller, *Journal of Bacteriology*, 1988, **170**, 3499-3508.

49. R. Hirsch, T. Ternes, K. Haberer and K.-L. Kratz, *Science of the Total Environment*, 1999, **225**, 109-118.

50. R. Hirsch, T. A. Ternes, K. Haberer, A. Mehlich, F. Ballwanz and K.-L. Kratz, *Journal of Chromatography A*, 1998, **815**, 213-223.

51. G. Artiaga, K. Ramos, L. Ramos, C. Cámara and M. Gómez-Gómez, *Food Chemistry*, 2015, **166**, 76-85.

52. T. Silva, L. R. Pokhrel, B. Dubey, T. M. Tolaymat, K. J. Maier and X. Liu, *Science of the Total Environment*, 2014, **468**, 968-976.

53. J. Trevisan, P. P. Angelov, A. D. Scott, P. L. Carmichael and F. L. Martin, *Bioinformatics*, 2013, 29, 1095-1097.

54. F. L. Martin, M. J. German, E. Wit, T. Fearn, N. Ragavan and H. M. Pollock, *Journal of Computational Biology*, 2007, **14**, 1176-1184.

55. M. Paraskevaidi, C. L. M. Morais, K. M. G. Lima, J. S. Snowden, J. A. Saxon, A. M. T. Richardson, M. Jones, D. M. A. Mann, D. Allsop, P. L. Martin-Hirsch and F. L. Martin, *Proceedings of the National Academy of Sciences USA*, 2017, **114,** E7929-E7938.

56. M. J. Riding, F. L. Martin, J. Trevisan, V. Llabjani, I. I. Patel, K. C. Jones and K. T. Semple, *Environmental Pollution*, 2012, **163**, 226-234.

57. J. Li, G. G. Ying, K. C. Jones and F. L. Martin, *Analyst*, 2015, **140**, 2687-2695.

58. I. Sondi and B. Salopek-Sondi, *J. Colloid Interface Sci.*, 2004, **275**, 177-182.
59. F. Pomati, A. G. Netting, D. Calamari and B. A. Neilan, *Aquatic Toxicology*, 2004, **67**, 387-396.
60. Z. Movasaghi, S. Rehman and D. I. ur Rehman, *Applied Spectroscopy Reviews*, 2008, **43**, 134-179.
61. J. C. Betts, P. T. Lukey, L. C. Robb, R. A. McAdam and K. Duncan, *Molecular Microbiology*, 2002, **43**, 717-731.
62. T. Hampshire, S. Soneji, J. Bacon, B. W. James, J. Hinds, K. Laing, R. A. Stabler, P. D. Marsh and P. D. Butcher, *Tuberculosis*, 2004, **84**, 228-238.
63. D. Schnappinger and W. Hillen, *Archives of Microbiology*, 1996, **165**, 359-369.
64. G. D. Shockman, J. J. Kolb and G. Toennies, *Journal of Biological Chemistry*, 1958, **230**, 961-977.
65. C. Marambio-Jones and E. M. Hoek, *Journal of Nanoparticle Research*, 2010, **12**, 1531-1551.
66. O. Gordon, T. V. Slenters, P. S. Brunetto, A. E. Villaruz, D. E. Sturdevant, M. Otto, R. Landmann and K. M. Fromm, *Antimicrobial Agents and Chemotherapy*, 2010, **54**, 4208-4218.
67. A. J. Kowaltowski and A. E. Vercesi, *Free Radical Biology and Medicine*, 1999, **26**, 463-471.
68. J. F. Turrens, *Bioscience Reports*, 1997, **17**, 3-8.
69. Y. Liu and J. A. Imlay, *Science*, 2013, **339**, 1210-1213.
70. I. Keren, Y. Wu, J. Inocencio, L. R. Mulcahy and K. Lewis, *Science*, 2013, **339**, 1213-1216.
71. H. H. Lara, N. V. Ayala-Núñez, L. d. C. Ixtepan Turrent and C. Rodríguez Padilla, *World Journal of Microbiology and Biotechnology*, 2010, **26**, 615-621.
72. Z.-M. Xiu, J. Ma and P. J. Alvarez, *Environ Sci Technol*, 2011, **45**, 9003-9008.
73. J. R. Morones, J. L. Elechiguerra, A. Camacho, K. Holt, J. B. Kouri, J. T. Ramírez and M. J. Yacaman, *Nanotechnology*, 2005, **16**, 2346.

598 74. D. Trachootham, Y. Zhou, H. Zhang, Y. Demizu, Z. Chen, H. Pelicano, P. J.
599 Chiao, G. Achanta, R. B. Arlinghaus and J. Liu, *Cancer Cell*, 2006, **10**,
600 241-252.

601

602

603 ## Figure Cations

604 **Figure 1.** Growth curves of *M. vanbaalenii* (A) and *P. fluorescens* (B) under AgNP,
605 tetracycline and AgNP-tetracycline binary exposures. The exposure concentrations
606 were 4 μg/L for AgNP and 1 μg/L for tetracycline. IR spectral average of *M.*
607 *vanbaalenii* (C) and *P. fluorescens* (D) in different exposure treatments. The groups
608 of "Log control", "Log silver", "Log tet" and "Log binary" refer to samples collected
609 at log-phase following treatments of control, silver, tetracycline and binary-exposure,
610 respectively.

611 **Figure 2.** Exposure effects within different growth phases (scale range of Y axis: -0.2
612 ~ 0.2). The Y axis refers to the values of LD1. *M. vanbaalenii*: control (A),
613 post-exposure to AgNP (B), post-exposure to tetracycline (C), and post-exposure to
614 AgNP-tetracycline mixture (D). *P. fluorescens*: control (E), post-exposure to AgNP
615 (F), post-exposure to tetracycline (G), and post-exposure to AgNP-tetracycline
616 mixture (H).

617 **Figure 3.** Vector-cluster analysis of exposure effects within different growth phases.
618 *M. vanbaalenii*: control (A), post-exposure to AgNP (B), post-exposure to tetracycline
619 (C), and post-exposure to AgNP-tetracycline mixture (D). *P. fluorescens*: control (E),
620 post-exposure to AgNP (F), post-exposure to tetracycline (G), and post-exposure to
621 AgNP-tetracycline mixture (H).

622 **Figure 4.** Exposure effects within the same growth phase. The Y axis refers to the
623 values of LD1 in range of -0.2 to 0.2. *M. vanbaalenii*: log-phase (A), stationary-phase
624 (B), and death-phase (C). *P. fluorescens*: log-phase (D), stationary-phase (E), and
625 death-phase (F).

626 **Figure 5.** Multivariate regression tree (MRT) analysis of environmental variables
627 explaining the discriminating biomarkers. The scale of the sub-figures represents the
628 alteration degree (1.0 refers to the average level). Blue bars for wavelengths
629 representing proteins, yellow bars for phospholipid-derived fatty acids, and grey bars
630 for other cellular components.

631 **Figure 6.** Vector-cluster analysis of exposure effects within the same growth phase.
632 *M. vanbaalenii*: log-phase (A), stationary-phase (B), and death-phase (C). *P.*
633 *fluorescens*: log-phase (D), stationary-phase (E), and death-phase (F).

634 **Figure 7.** Ratio of cysteine (CySS, 668 cm^{-1}) to protein (1447 cm^{-1}) derived from
635 Raman spectra. Data are presented in mean ± standard error.

636

637 **Figure 1**

638

639

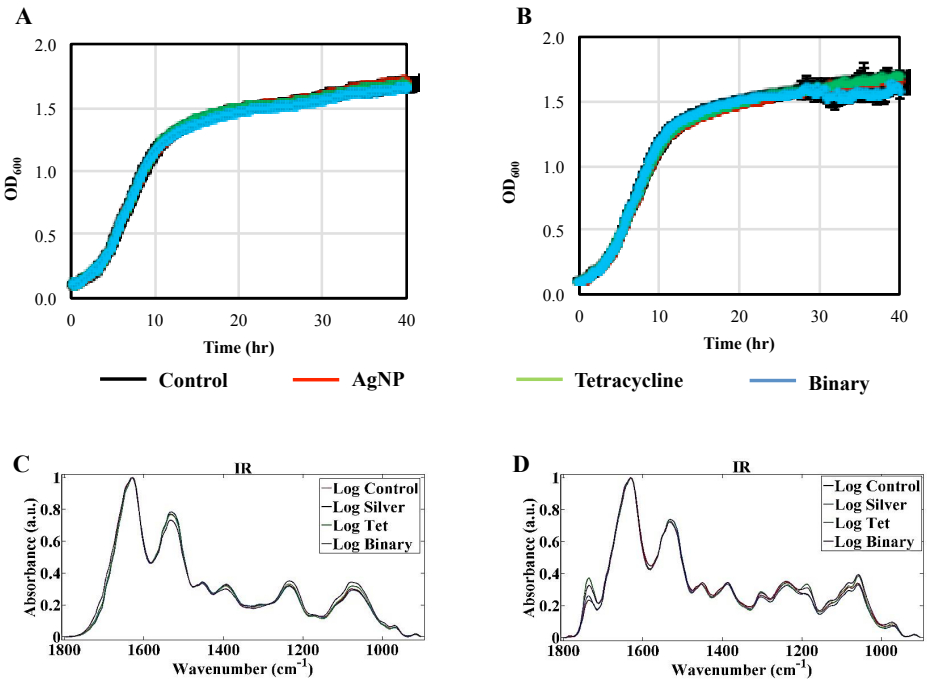

640

641 **Figure 2**

642

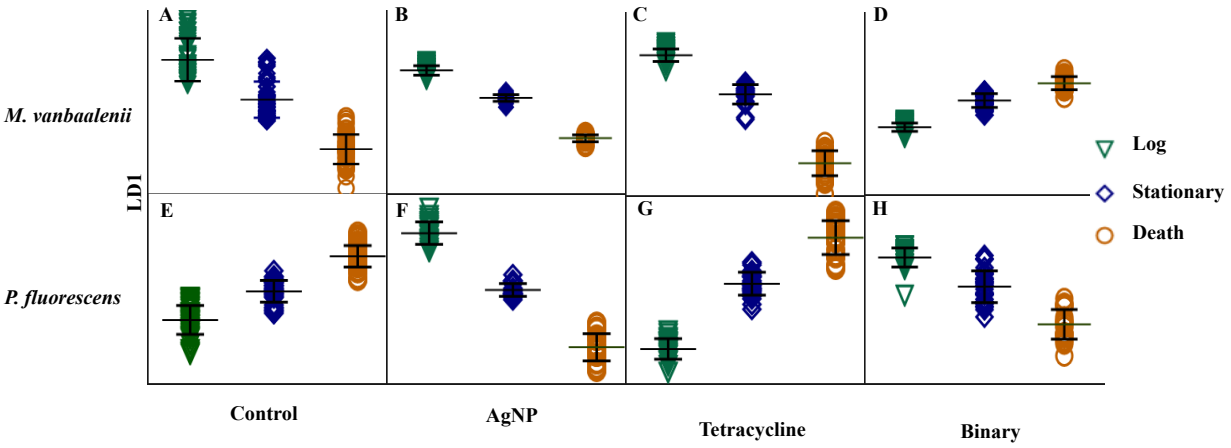

643

644

645 **Figure 3**

646

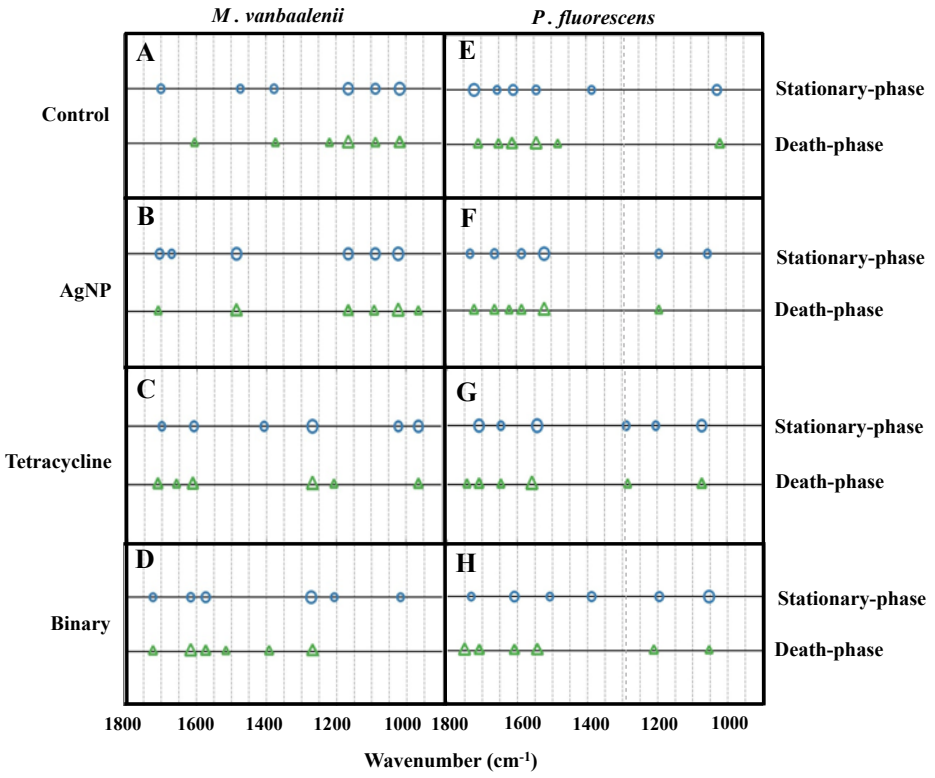

647

648

649 **Figure 4**

650

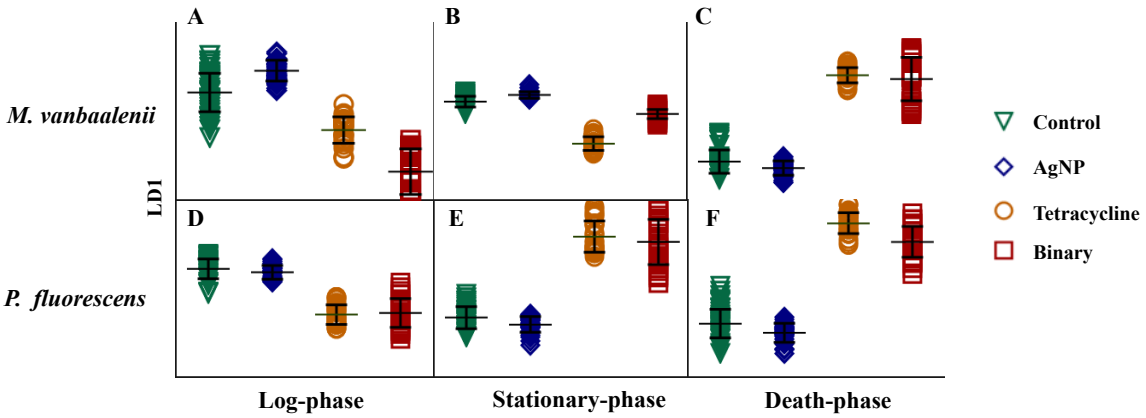

651

652

653 **Figure 5**

654

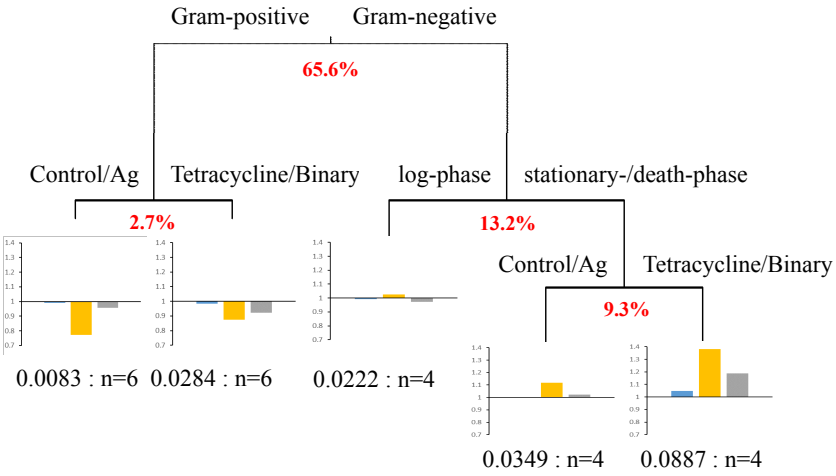

655

Error: 0.0924 CV Error: 0.295 SE: 0.118

656

657 **Figure 6**

658

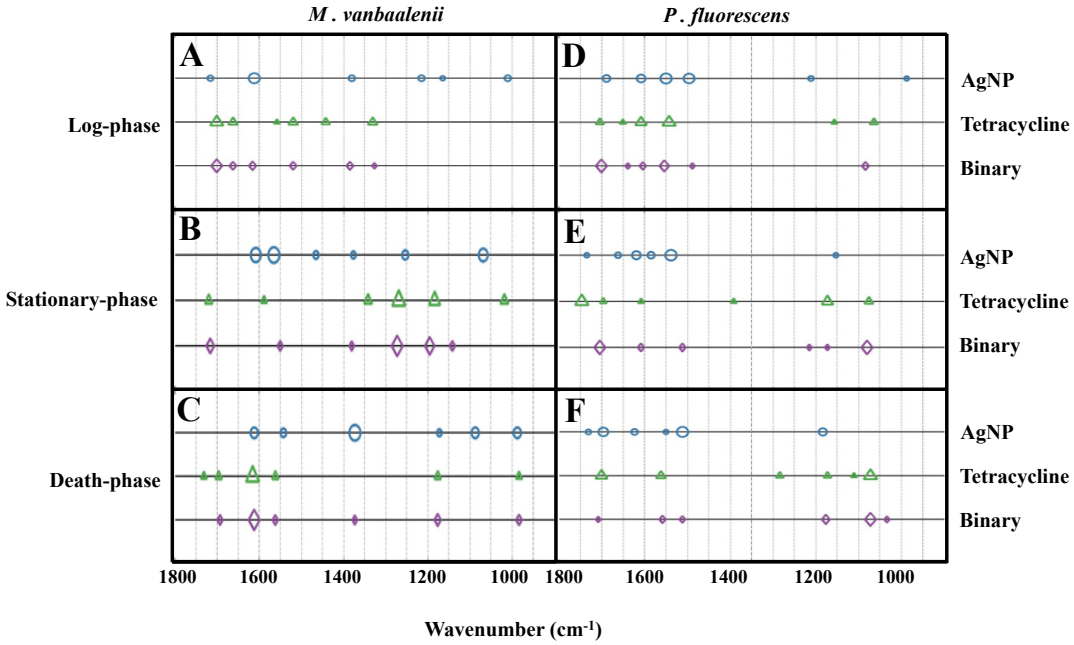

659

660

661 **Figure 7**

662

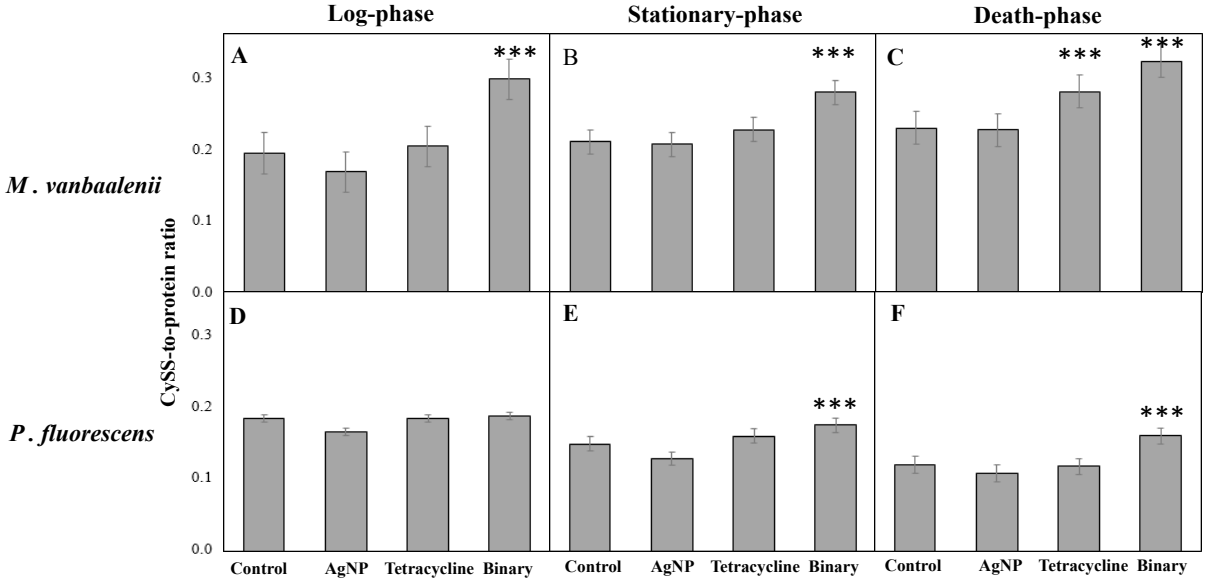

663